

**Decomposing satellite-based rainfall errors in flood estimation
Hydrological responses using a spatiotemporal object-based verification method**

Laverde-Barajas, M.; Corzo Perez, G. A.; Chishtie, F.; Poortinga, A.; Uijlenhoet, R.; Solomatine, D. P.

DOI

[10.1016/j.jhydrol.2020.125554](https://doi.org/10.1016/j.jhydrol.2020.125554)

Publication date

2020

Document Version

Final published version

Published in

Journal of Hydrology

Citation (APA)

Laverde-Barajas, M., Corzo Perez, G. A., Chishtie, F., Poortinga, A., Uijlenhoet, R., & Solomatine, D. P. (2020). Decomposing satellite-based rainfall errors in flood estimation: Hydrological responses using a spatiotemporal object-based verification method. *Journal of Hydrology*, 591, 1-13. Article 125554. <https://doi.org/10.1016/j.jhydrol.2020.125554>

Important note

To cite this publication, please use the final published version (if applicable).
Please check the document version above.

Copyright

Other than for strictly personal use, it is not permitted to download, forward or distribute the text or part of it, without the consent of the author(s) and/or copyright holder(s), unless the work is under an open content license such as Creative Commons.

Takedown policy

Please contact us and provide details if you believe this document breaches copyrights.
We will remove access to the work immediately and investigate your claim.

Green Open Access added to TU Delft Institutional Repository

'You share, we take care!' - Taverne project

<https://www.openaccess.nl/en/you-share-we-take-care>

Otherwise as indicated in the copyright section: the publisher is the copyright holder of this work and the author uses the Dutch legislation to make this work public.



Research papers

Decomposing satellite-based rainfall errors in flood estimation: Hydrological responses using a spatiotemporal object-based verification method

M. Laverde-Barajas^{a,b,*}, G.A. Corzo Perez^a, F. Chishtie^{c,d}, A. Poortinga^{c,d}, R. Uijlenhoet^e, D.P. Solomatine^{a,b}

^a IHE-Delft Institute for Water Education, Westvest 7, 2611 AX 2611 Delft, The Netherlands

^b Delft University of Technology, 2628 CN Delft, The Netherlands

^c Spatial Informatics Group, LLC, 2529, Yolanda Ct., Pleasanton, CA 94566, USA

^d SERVIR-Mekong, SM Tower, 24th Floor, 979/69 Paholyothin Road, Samsen Nai Phayathai, Bangkok 10400, Thailand

^e Wageningen University, Nieuwe Kanaal 11, 6709 PA Wageningen, The Netherlands

ARTICLE INFO

This manuscript was handled by Emmanouil Anagnostou, Editor-in-Chief

Keywords:

Satellite-based rainfall
Spatiotemporal error analysis
Object-based method
Hydrology
Storm

ABSTRACT

A spatiotemporal object-based rainfall analysis method is used to evaluate the hydrological response of two systematic satellite error sources for storm estimation in the Capivari catchment, Brazil. This method is called Spatiotemporal Contiguous Object-based Rainfall Analysis (ST-CORA) specifically evaluates the error structure of satellite-based rainfall products using a 3D pattern clustering algorithm. Errors due to location and magnitude in the Near Real-time (NRT) CMORPH product are subtracted by adjusting the shift and the intensity distribution with respect to a storm object obtained from gauge-adjusted weather radar. Synthetic scenarios of each error source are used as forcing for hourly calibrated distributed hydrological 'wflow-sbm' model to evaluate the main sources of systematic errors in the hydrological response. Two types of storm events in the study area are evaluated: short-lived and a long-lived storm. The results indicate that the spatiotemporal characteristics obtained by ST-CORA clearly reflect the main source of errors of the CMORPH storm detection. It is found that location is the main source of error for the short-lived storm event, while volume is the main source in the long-lived storm event. The subtraction of both errors leads to an important reduction of the simulated streamflow in the catchment. The method applied can be useful in bias correction schemes for satellite estimations especially for extreme precipitation events.

1. Introduction

The spatiotemporal characteristics of storm events, such as magnitude, duration and spatial extent, are some of the main triggering factors of flooding. In conjunction with intrinsic characteristics of the catchment, changes in the storm structure can dramatically impact the severity of flood damage [e.g. Saulnier and Le Lay (2009), Bui et al. (2014), Viglione et al. (2010)]. Therefore, an accurate representation of storm dynamics is crucially important in disaster preparedness and response (Phongsapan et al., 2019). However, in prominent monsoon regions, the high spatial and temporal variability of storm events still makes the estimation challenging.

A great deal of effort has been made to provide rainfall measurements with high spatial and temporal resolution. Traditionally, rain-gauge measurements were used since they are the most simple and direct method for measuring of rainfall. However, in many regions, rain

gauge networks are often scarce, discontinuous and not dense enough to accurately capture the spatiotemporal variation in rainfall (Michaelides et al. (2009); Tolentino et al., 2016; Kidd et al., 2017). Recently, satellite-based rainfall products (SRP) have widely used in hydrological applications for overcoming the lack of spatial representation of rain-gauges [e.g.] Artan et al. (2007), Nikolopoulos et al. (2013), Stisen and Sandholt (2010), Su et al. (2008). A variety of global-scale satellite-derived rainfall products are freely and openly. Sun et al. (2018) presented a full description of operational and non-operational SRP.

Despite numerous advances, satellite products are subject to several systematic and random errors from multiple sources [e.g.] Hu et al. (2016), Qiao et al. (2014), Dinku et al. (2010), Guo et al. (2015), Mei et al. (2014), Sapiano and Arkin (2009), Thiemi et al. (2012), Poortinga et al. (2017). These errors have several implications in relation to their input for modelled flood response [e.g.] Casse et al.

* Corresponding author.

E-mail address: m.laverde@un-ihc.org (M. Laverde-Barajas).

(2015), Bitew and Gebremichael (2011), Mei et al. (2016), Vergara et al. (2014), Yilmaz et al. (2005), Li et al. (2009). Maggioni and Massari (2018), analysing the lessons from using satellite precipitation products for riverine flood modelling around the world, argued that the performance of SRP-forced hydrological model depends on several factors including: the type of SRP sensor; the precipitation type; the geomorphological conditions; and the hydrological model formulation.

In general, satellite error studies use pixel-based verification metrics such as categorical or continuous metrics to calculate the differences between pixels SRP and the corresponding ground measurement. Based on this approach, error models have been developed to quantify the systematic and random error distribution and to propagate their uncertainty in the streamflow [e.g.] Hossain and Anagnostou (2006), Maggioni et al. (2014), Falck et al. (2015). While these outputs provide valuable information about bias and correlation between SRP errors, such metrics do not explicitly estimate errors associated with location, spatial representation and geometrical patterns (Baldwin and Kain, 2006; Casati et al., 2008). Several analytical methods have been used to analyse the error decomposition in satellites and evaluate the spatiotemporal dynamics in terms of streamflow [e.g.] Viglione et al. (2010), Mei et al. (2017), Mei et al. (2017). However, the error decomposition is limited by the configuration of the hydrological model. In contrast to analytical methods, rainfall object-based methods aim to represent the cells and integrate spatiotemporal information from an event as an interconnected mass figure which can be used to characterise the storm events. These object-based methods offer an alternative way to analyse the error in storm events [e.g.] Skok et al. (2009), Li et al. (2015), Li et al. (2016). These methods, applied in hydrological modelling, can be used to evaluate the impact of several systematic SRP errors in forecasted streamflow, independently of the model configuration. For example, Demaria et al. (2011) used the Contiguous Rainfall Analysis (CRA, Ebert and McBride (2000)) to evaluate the hydrological impact of location errors presented in three SRP namely Tropical Rainfall Measurement Mission (TRMM), Climate Prediction Centre Morphing Technique (CMORPH), and Precipitation Estimation from Remotely Sensed Information using Artificial Neural Networks (PERSIANN). The analysis showed that errors due to location represented more than 65% of the total errors affecting the peak of the streamflow, thus also its volume.

Important challenges in object-based methods arise from the effect of displacements calculated in space and time. The two-dimensional approach of existing methods limits the description of the storm event in space and time. Several methods have considered the spatiotemporal dynamic of the storm event. For instance (Davis et al., 2009) developed a Method for Object-based Diagnostic Evaluation with Time Domain (MODE-TD) to evaluate the forecast of high-resolution numerical weather prediction models. This model was later evaluated by Mittermaier and Bullock (2013) over the United Kingdom outperforming spatial object-based methods. For satellite-based products, Sellars et al. (2013) developed a spatiotemporal rainfall analysis using PERSIANN to create the four-dimensional global dataset – PERSIANN-CONNECT. This product identifies the main characteristics of large scale rainfall systems. In the case of spatiotemporal analyses at catchment scale, Laverde-Barajas et al. (2019) developed a spatiotemporal object-based method, later named ST-CORA (Spatiotemporal Contiguous Object-based Rainfall Analysis). ST-CORA, a three-dimensional object-based approach influenced by pattern recognition methods for global data analysis [e.g.] Corzo Perez et al. (2011), is designed to analyse errors resulting from satellite estimation as a consequence of displacement, magnitude or pattern effects (Ebert and McBride, 2000). This method performed well in identifying the main characteristics of convective storm events.

In this study, we used the ST-CORA method to evaluate the hydrological impact of two systematic errors in the near real-time CMORPH for storm event estimation: the error due to location and that due to magnitude. Synthetic storm scenarios, created by the subtraction

of location and magnitude error sources, are propagated through the distributed hydrological model wflow-sbm (Schellekens et al., 2018) in the subtropical catchment of the Capivari River, Brazil. The model is calibrated at an hourly scale during 2016 using a gauge-corrected weather radar as reference data. Two types of storm event are analysed: local and short events (short-lived storms) and long duration, spatially extensive, extreme events (long-lived storms). We believe that this approach can contribute to a better understanding of the hydrological response to systematic errors in SRPs, especially in extreme conditions.

The paper is structured as follows: in Section 2, we describe the formulation of ST-CORA and the methodology used for error source subtraction and the hydrological response evaluation. In Section 3, the study area and data availability is outlined. Section 4 presents the hydrological model as well as the calibration and validation process. In Section 5, results regarding the error subtraction and error propagation in the study area are presented. Section 6 discusses the results, and finally, Section 7 presents the conclusions and the analysis of future directions.

2. Methodology

2.1. Rainfall object estimation, ST-CORA

ST-CORA is a spatiotemporal object-based method designed to analyse the spatiotemporal characteristics of different storm events at catchment scale (duration, spatial extent, magnitude, and centroid). This method uses a multidimensional connected-component labelling algorithm to detect regions with similar features in space and time. The error verification for SRP allows the error decomposition in displacement, volume and pattern error. The methodology for error verification is composed of three steps, briefly described below.

2.1.1. Identification of spatiotemporal convective objects

In this step, the method identifies convective rainfall objects using a multidimensional connected-component labelling algorithm (Acharya and Ray, 2005; Sedgewick, 1998). This object is defined as a group of voxels (volume representation of a pixel) connected by a rainfall intensity threshold $S_{[x,y,t]}$ (1 = “true” or 0 = “false”) (Eq. 1).

$$S_{[x,y,t]} := \begin{cases} 1, & \text{if } R_{x,y,t} \geq IT. \\ 0, & \text{otherwise.} \end{cases} \quad (1)$$

where, $R_{x,y,t}$ is the rainfall voxel and IT is the rainfall intensity threshold. Once all $S_{[x,y,t]}$ voxels have been determined, the algorithm scans all voxels in a neighbouring system (from top to bottom and from left to right) and groups voxels with similar features by assigning preliminary labels to $S_{[x,y,t]}$ as

$$c(S_{[x,y,t]}) = \{N_{[x,y,t]} \in \alpha s: S_{CR} = S_N\} \quad (2)$$

where, $c(S_{[x,y,t]})$ is a preliminary label, S_{CR} , S_N are binary properties of the voxel $S_{[x,y,t]}$ and its neighbours $N_{[x,y,t]}$ respectively, and αs is the neighbour system in space and time. The labelling process $c(S_{[x,y,t]})$, is repeated for resolving the equivalences of labels across the different regions during the grouping phase.

After obtaining the convective rainfall object, the methodology applies two error filtering algorithms to remove small noisy objects and solves the false merging errors from the connected-component labelling algorithm. In the first instance, a size-filtering algorithm removes objects lower than a size threshold, T , defined as noise (Ceperuelo et al., 2006). In this study, we defined noise to objects lower than four connected voxels in space and time (voxel = 0.1°/h). The second algorithm removes false merging errors, which are created when two individual storm events are identified as a single storm. To overcome this error, ST-CORA uses a closing algorithm morphology to delineate and segment convective objects. Using a dilation-erosion process, this algorithm divides or merges convective objects with low or strong

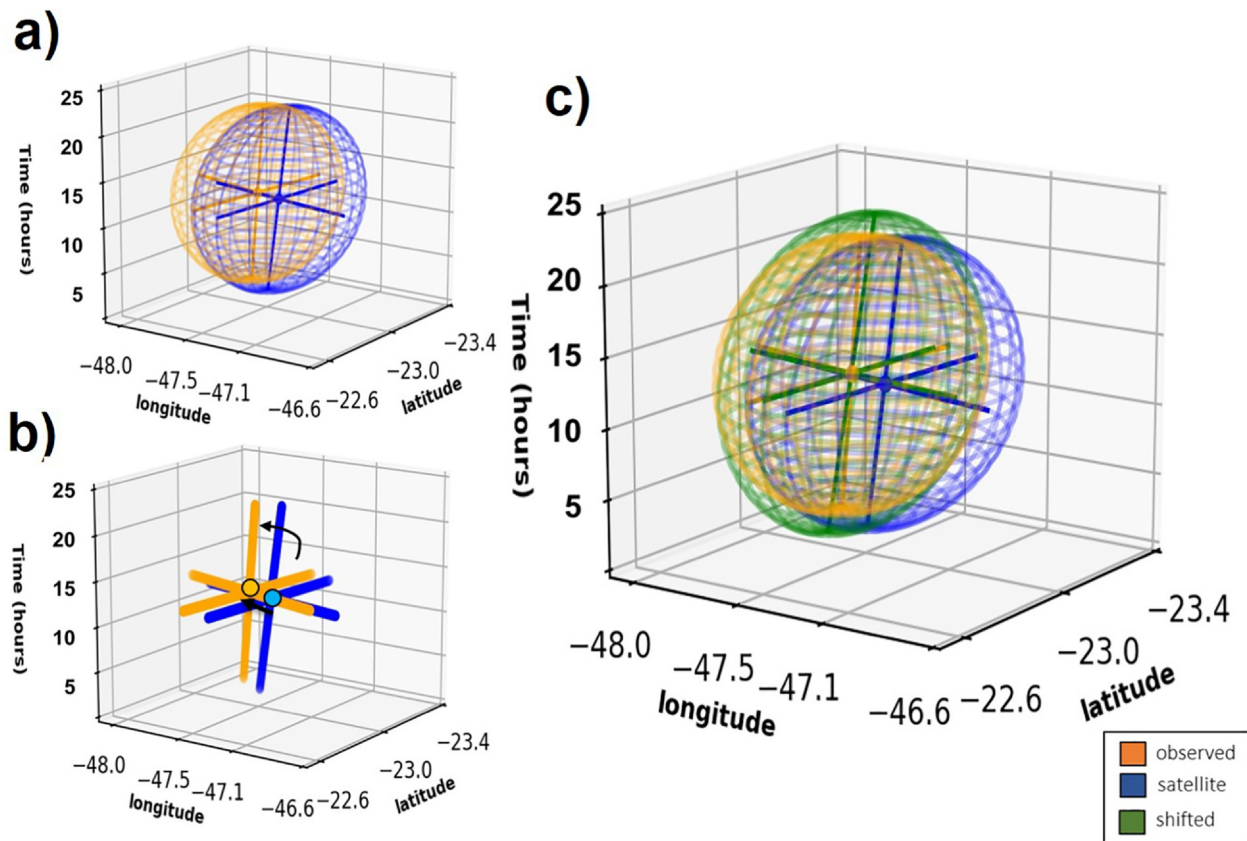


Fig. 1. Scheme of object matching for location subtraction. a) Eigenvectors of a compressed the storm object b) weighted centroid and eigenvector matching. c) Shifted storm object.

connectivity [e.g.] Han et al. (2009). For dilation, object boundaries are expanded, whilst for erosion, those boundaries are removed.

2.1.2. Storm segmentation and classification

In the second step, the storm is segmented and classified on basis of the spatiotemporal properties of the convective object. In ST-CORA, storm events are defined according to the Critical Mass Threshold (CMT) (Grams et al., 2006). This parameter corresponds to the minimum volume of a convective rainfall object that is required in order to be considered an extreme event. The CMT value is obtained from the relationship between the maximum extent and object volume (Steiner et al., 1995; Demaria et al., 2011). Once the storm event is identified, the spatiotemporal properties are used to classify the type of storm event. Following hydrometeorological and dynamical criteria to classify severe rainfall events proposed by Molini et al. (2009), Molini et al. (2011), Boers et al. (2015), ST-CORA classifies storm events in two groups depending on the maximum area, the storm duration and the volume of rainfall: small convective systems with a short duration (short-lived) and long duration systems extended over large areas (long-lived).

In ST-CORA, the definition of (IT) and critical mass threshold (CMT) are important parameters which help to identify and segment storm events. Based on the sensitivity analysis made by Laverde-Barajas et al. (2019) in the region, we selected an IT of 1 mm/h and a CMT of 0.01 km³ to identify and segment extreme convective objects. Based on the spatiotemporal characteristics of extreme rainfall events presented by Laverde-Barajas et al. (2018), Laverde-Barajas et al. (2019) in the study area, we defined short-lived events as extreme convective objects with a duration of less than 12 h and spatial distribution greater than 86 × 86 km²

2.1.3. Spatiotemporal verification

The last step corresponds to the error verification analysis. In this step, observed and estimated SRP storm objects are compared to evaluate the error level for storm estimation. In ST-CORA, several error metrics can be evaluated to estimate the error. In this study, we used the error decomposition from the Contiguous Rainfall Analysis method (CRA) developed by Ebert and McBride (2000). This method analyses the spatial elements of the SRP error decomposing the total error into displacement, volume and pattern error as shown below.

$$MSE_{total} = MSE_{displacement} + MSE_{volume} + MSE_{pattern} \tag{3}$$

where

$$MSE_{displacement} = MSE_{total} - MSE_{location} \tag{4}$$

$$MSE_{volume} = (\bar{Y} - \bar{O})^2 \tag{5}$$

$$MSE_{pattern} = MSE_{location} - MSE_{volume} \tag{6}$$

where $MSE_{location}$ is calculated as the mean square error of the spatial shifted SRP and \bar{Y} and \bar{O} are the mean satellite and observed values after the shift. In the context of satellite-based rainfall data, $MSE_{displacement}$ and MSE_{volume} are considered as systematic errors, while $MSE_{pattern}$ corresponds to intrinsic random errors in the measurements, which are calculated as the residual error of systematic errors (Hoffman et al., 1995; Ebert and Gallus, 2009). It is important to highlight that systematic errors integrate random error as a consequence of non-corrected values from location and magnitude subtraction. In this research, we considered non-corrected error as part of pattern error in the storm event.

2.2. Systematic error source subtraction

The use of ST-CORA allows for the temporal and spatial description

of storm events as well as for identifying the main sources of error in the measurement. Once the main storm characteristics are identified (volume, maximum intensity, max area and duration), we subtracted location error as the main source in displacement and magnitude as the main source of volume by the following approach.

2.2.1. Location subtraction

Location is subtracted by finding the best match between the observed and the satellite storm. In this research, we used the Principal Component Analysis method (PCA) proposed by Johnson and Hebert (1999), to remove the shifting and orientation effects of the satellite storm in space and time (Grams et al., 2006) (Fig. 1). PCA is a statistical method that describes the pattern of multi-variable data based on orthogonal variables called principal components (Abdi and Williams, 2010). Based on an ellipsoid wrapped over the object with weighted-centroid (WC), the methodology calculates the eigenvectors of the object (Fig. 1a). These vectors describe the orthogonal basis in space and time, in which the object position is described (Johnson and Hebert, 1999). Location error subtraction first removes the shifting effect by matching the weighted-centroids of both objects in space and time and then the orientation is adjusted by rotating the temporal eigenvector in the direction of the observed vector (Fig. 1b, c).

2.2.2. Magnitude subtraction

The magnitude subtraction statistically adjusts all moments (quantiles) of the intensity probability distribution function for the satellite storm with respect to the observed storm. In this case, the adjusted satellite storm intensity distribution should reflect the function of the observed storm. Several methodologies have been developed to equalise the histograms and remove the bias from the estimated data [e.g. Cannon et al. (2015), Themeßl et al. (2012), Teng et al. (2015)]. For this research, we selected the extensively used Empirical Quantile Mapping method (EQM) (Themeßl et al., 2012). This method adjusts all moments of the cumulative probabilistic function (*ecdfs*) of the satellite in terms of intensity with respect to the observed data. The relationship between the *ecdf* for observed (*ecdf_{obs}*) and the satellite (*ecdf_{sat}*) is based on the following equation:

$$EGM = ecdf_{obs}^{-1}(ecdf_{sat}^{-1}(I_s)) \quad (7)$$

where, I_s is the intensity storm distribution detected by the satellite.

Once the magnitude error source is subtracted, the volume equation, Eq. 5, can be reformulated to included the magnitude subtraction as follows:

$$MSE_{volume} = MSE_{total} - MSE_{magnitude} \quad (8)$$

2.3. Evaluation of the hydrological response

Synthetic scenarios, created by the individual subtraction of location and magnitude error sources from storm events detected by satellites, are propagated through a hydrological model to evaluate the error response in terms of stream-flow. The hydrological response is evaluated by comparing simulations from satellite scenarios against simulations from observed rainfall. We used several metrics to analyse the shape, phase and amplitude of the stream-flow along the catchment. These metrics include the correlation coefficients (r), Root Mean Square Error (*RMSE*), the Mean Absolute Peak Time Error (*MAPTE*) (Ehret and Zehe, 2011), Percentage Peak Effect index (*PPE*) and the Percentage Volume Effect (*PVE*) (Bennett et al., 2013).

$$r = \frac{\sum_{t=1}^N \left(Q_{rad,t} - \overline{Q_{rad}} \right) \left(Q_{sat,t} - \overline{Q_{sat}} \right)}{\sqrt{\sum_{t=1}^N \left(Q_{rad,t} - \overline{Q_{rad}} \right)^2} \sqrt{\sum_{t=1}^N \left(Q_{sat,t} - \overline{Q_{sat}} \right)^2}} \quad (9)$$

$$RMSE = \sqrt{\frac{1}{N} \sum_{t=1}^N \left(Q_{rad,t} - Q_{sat,t} \right)^2} \quad (10)$$

$$MAPTE = \frac{1}{N} \sum_{t=1}^N \left| P_{rad,t} - P_{sat,t} \right| \quad (11)$$

$$PPE = \frac{Q_{rad,max} - Q_{sat,max}}{Q_{rad,max}} * 100 \quad (12)$$

$$PVE = \frac{V_{rad} - V_{sat}}{V_{rad}} * 100 \quad (13)$$

Here, $Q_{rad,max}$ and $Q_{sat,max}$ are the maximum discharge simulated by the radar (referenced value), and the satellite discharge values (original, location and magnitude) for each discharge station. $P_{rad,t}$ and $P_{sat,t}$ are the peak times and V_{rad} and V_{sat} are the simulated total volume based on the radar and the satellite, respectively.

The streamflow error variation between CMORPH and the location and magnitude scenarios for the short- and long-lived storms, is evaluated by the following equation:

$$Errorvariation_t = \frac{Q_{sat,t} - Q_{rad,t}}{Q_p} * 100 \quad (14)$$

where, Q_p is the maximum discharge value reached in all storm scenarios.

3. Case study and data availability

3.1. Study area

The study area corresponds to the subtropical catchment of the Capivari River in south-eastern Brazil (Fig. 2). This river is a tributary of the Tiete River which is part of the Parana area, one of the main river systems in Brazil. The drainage area is 1655 km² and the elevations range from 400 to 1000 m above sea level. The catchment experiences extreme climatological conditions, such induced by the convective precipitation band associated with the South American Monsoon System, making the study area prone to landslides and flash floods (Swiss, 2011). We divided the catchment into three zones: upper, middle, and lower. The upper zone is localised to the east part of Campinas city, ending at the flow station at the boundary of the city. This zone is characterised by semi-urbanised areas extended over an elevated landscape. The middle zone is located upstream the Monte gauge station, and is covered by the urban area of Campinas city, which is the main urban centre of the catchment. Finally, the lower zone is located upstream of the streamflow outlet to the Tiete River and corresponds to rural and semi-rural areas of lower elevations.

Based on the Integrated Disaster Database system from National Civil Protection Secretary (S2ID, SEDEC (2013)), we selected a short-lived and long-lived storm event that impacted the Capivari basin during monsoon season. The short-lived event was a high convective storm that occurred on 1 January 2012. According to S2ID database, the extreme rainfall from this event generated important pluvial floods in urban areas along the catchment and initiated the overflowing (alagamiento) of the Capivari river. The event corresponding to the long-lived storm impacted the study area between 3 and 5 January 2011. This event dramatically impacted the area, triggering extensive floods and landslides over the region.

3.2. Rainfall data

In this study, we used the CPC MORPHING product (CMORPH) developed by the NOAA Climate Prediction Centre (Joyce et al., 2004). This SRP combines Passive Microwave and Infrared sensor information to produce high resolution data every 30 min. CMORPH NRT was selected due to a superior performance for extreme rainfall estimation in

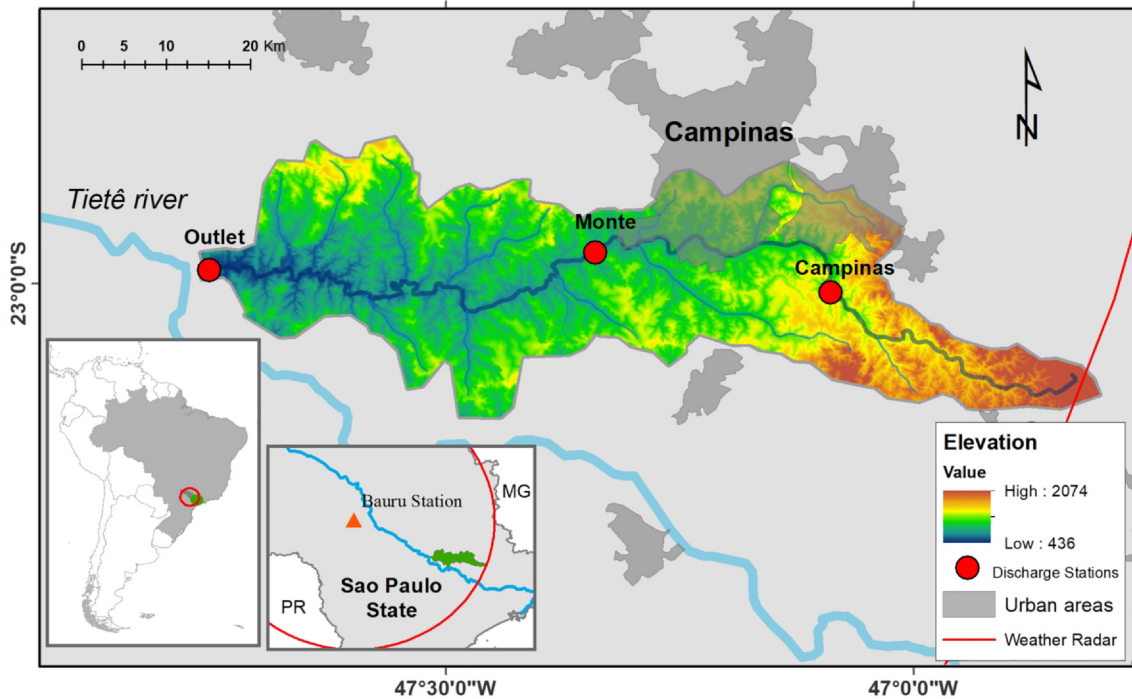


Fig. 2. Geographical location of the Capivari catchment. Red dots represent the discharge station of Campinas, Monte and the virtual station in Outlet. Red cycled represent the weather radar Bauru used as ground measurements. (For interpretation of the references to colour in this figure legend, the reader is referred to the web version of this article.)

the study area (Laverde-Barajas et al., 2018). We used CMORPH 1.0 raw version at 8×8 km scale (0.727 degrees) and 30 min resolution (1 h aggregated).

Ground measurements were obtained from the Bauru weather radar station (Bauru CAPPI 3.5 km) from the Faculty of Science, Sao Paulo State University located at $22^{\circ}21'28''S$ latitude, $49^{\circ}01'36''W$ longitude (Fig. 1). This radar provides information at 1 km^2 spatial resolution every 15 min. Weather radar rainfall data was bias-corrected at hourly scale using 8 automatic ground stations from the Integrated Centre of Agrometeorological information (CIIAGRO, Centro Integrado de Informações Agrometeorológicas) applying the mean fields reduction described in Amorati et al. (2012) (Eq. 15)

$$R_{merged} = RF, \tag{15}$$

where, R is hourly rainfall field and F is the weighted correction factor with temporal averaged windows, Δt , calculated as follows:

$$\overline{\log F}_t = \frac{\sum_{\tau=t-\Delta t}^t \sum_{i=1}^{N_r} \log_{10} \left(\frac{G_{i,t}}{R_{i,t}} \right)}{\sum_{\tau=t-\Delta t}^t N_r}, \tag{16}$$

where, G_i and R_i are the Automatic Weather Stations (AWS) and radar measurements at gauge i , respectively. A three-hour temporal window, Δt , is considered for the $\overline{\log F}_t$. In order to reduce the effect of differences in the spatial resolution (Pelegrino et al., 2018), we scaled up weather radar data by mean aggregation to match the spatial resolution of the CMORPH dataset.

4. Capivari model

We used distributed hydrological model wflow-sbm (version 2018.1), to represent the rainfall-runoff process in the Capivari River. This model was developed by project Deltares OpenStreams (Schellekens et al., 2018) based on the topog-sbm model (Vertessy and Elsenbeer, 1999). The wflow-sbm simulates the hydrological routing

through a gridded mesh into a GIS environment called PCRaster-Python (Wesselung et al., 1996).

The representation of the hydrological cycle within wflow-sbm is divided into the three main routines: interception, soil, and water surface. Wflow-sbm simulates interception using the analytical Gash model (Gash et al., 1995). This model calculates the actual evapotranspiration of the canopy based on the Potential Evapotranspiration (PET), soil water content and land cover type. The soil routine runs per grid cell through the topog-sbm model. This model is a simple bucket scheme designed to transfer the water infiltration process into a saturated (S) and unsaturated store (US). The S and US interaction is based on the exponential decay of the saturated hydraulic conductivity with depth below the soil surface (K_{sat}) (Schellekens et al., 2018). The surface water routine uses the kinematic wave algorithm to simulate the river drainage and overland flow. The runoff is calculated per grid cell as the sum of residual rainfall water from the interception and soil routines and the horizontal and vertical interaction between cells estimated in the routing process.

4.1. Model setup

For each rainfall data product, we setup the wflow-sbm model in a $1\text{ km} \times 1\text{ km}$ grid integrating several static and dynamic inputs. Static inputs are integrated by i) the Digital Elevation Model from the Shuttle Radar Topography Mission (SRTM) version 3.0 (Van Zyl, 2001); ii) land use map extracted from the Brazilian land use map of the National Institute of Geography and Statistics (IBGE, 2017) for 2014; and iii) the soil type map, extracted from the FAO Digital Soil Map of the World (DSMW-FAO, 1960).

In addition to the rainfall data, dynamic inputs are hourly air temperature (T) in degree Celsius and potential evapotranspiration (PET) maps based on the AWS from CIIAGRO (Fig. 2). PET is calculated using the method of Abtew (1996) recommended by Tangune and Escobedo (2018) for the study area. This method calculates PET in mm/h using the air temperature and solar radiation as

$$PET = \frac{0.53}{2.501 - 0.002361T}Rs, \tag{17}$$

where, Rs is the solar radiation data from AWS. Hourly T and PET data was interpolated using the Inverse Distance Weight method (IDW-2). This method is widely used in meteorology and it was selected for providing reliable hourly information based on the total number of available stations (Chung and Yun, 2004; Chen et al., 2019). However, it is noted that interpolation methods are subject to several sources of uncertainty due to the spatial sampling and geomorphological conditions in the catchment. These uncertainties include the misrepresentation between meteorological variables and elevation (DeGaetano and Belcher, 2007).

4.2. Model calibration and validation

Wflow-sbm requires 15 input parameters to be calibrated in the study area (excluding the input snow parameters). We calibrated the Capivari hydrological model using hourly discharge data from the Early Warning Flood System of Sao Paulo state (SAISP) available in the area, with the upper zone calibrated based on the Campinas station between January and October 2016. In the middle zone the model was calibrated based on the Monte station between July and October 2016. In the absence of hourly discharge data in the lower zone, the model was calibrated based on a virtual discharge point in the outlet area calculated using the spatiotemporal linear estimator proposed by Paiva et al. (2015):

$$\hat{Q}\left(S_o, t_o\right) = \sum_{i=1}^N \lambda_i Q\left(S_i, t_i\right) \tag{18}$$

Here, \hat{Q} is the virtual station at location S_o , Q are Campinas and Monte discharges and $\lambda = [\lambda_1, \dots, \lambda_n]^T$ is the set of weights for each measurement. For the study area, λ represents the relative drainage area of each discharge point. All areas were validated during the period of November and December 2016.

The calibration process started by adjusting the input parameters to the most realistic interval and then we selected the most sensitive ones using a Monte Carlo Analysis. Table 1 shows the most sensitive input parameters in the Capivari model. Using the Augmented Lagrangian Harmony Search Optimizer (ALSHO, (Geem et al., 2001)) from Perez et al. (2012), we calibrated the model for the three zones, from upstream to downstream, using the Nash-Sutcliffe efficiency (NSE, Nash and Sutcliffe (1970) as the objective function define as:

Table 1
Wflow-sbm parameters selected.

No	Parameter	Description	Interval
<i>Canopy interception</i>			
1	CanopyGapFraction	Fraction of precipitation that does not hit the canopy directly	[0–1]
<i>Soil</i>			
2	M	parameter in the SBM model. Governs the decay of Ksat with depth [–]	[20–20000]
3	thetaS	Saturated water content (porosity) [mm/mm]	[0.2–0.5]
4	KsatVer	Saturated conductivity [mm/h]	[0–10000]
5	Infiltr CapSoil	Soil infiltration capacity [m/h]	[25–750]
6	Soil Thickness	Maximum depth of the soil [m]	[0–20000]
<i>Surface Water</i>			
7	N	Manning’s N parameter	[0.02–0.15]
8	N _{river}	Manning’s N parameter for cells marked as river	[0.01–0.6]

$$NSE = 1 - \frac{\sum_{i=1}^N (Q_{obs,i} - Q_{sim,i})^2}{\sum_{i=1}^N (Q_{obs,i} - \overline{Q_{sim}})^2} \tag{19}$$

where, Q_{obs} and Q_{rad} are the model’s observed and simulated streamflow, respectively, using the gauge-corrected weather radar as the input.

Model calibration and validation were additionally compared with the Root Mean Square Error (RMSE) (Eq. 10) and correlation coefficient (r) (Eq. 9). Table 2 describes the model performance over the three zones based on NSE , $RMSE$, R . Model results displayed satisfactory results for estimating hourly streamflow along the catchment with NSE ranging between 0.6/0.5 and 0.8/0.6 in calibration/validation and having a correlation coefficient higher than 0.76 and $RMSE$ lower than 20 mm on the evaluated areas.

5. Results

5.1. Spatiotemporal errors of satellite-based CMORPH

5.1.1. Detecting systematic errors in satellite-based storm events using ST-CORA

Fig. 3 presents the object structure and storm properties of the reference radar and the satellite-based CMORPH identified by ST-CORA for the short-lived storm event that occurred on 1 January 2012 and, the long-lived storm event that occurred between 3 and 5 January 2011. Fig. 3a, b present storm objects of the radar and satellite-based CMORPH for the short-lived event, while Fig. 3d, e show the object structures for the long-lived event. Fig. 3c, f present the comparison of the scatter plots and the spatiotemporal properties of both objects for both storm events.

According to the results, radar and CMORPH exhibit similar spatiotemporal structures but differ in the magnitude and the location of the object. CMORPH performance for the short-lived event showed an underestimation on high intensity rain rates (Fig. 3c). However, the total storm volume was higher compared to the storm detected by the radar. The spatiotemporal properties are characterised by a mismatch in the orientation of the CMORPH event. Both objects have the same duration (7 h), and CMORPH reached a bigger spatial extension. The satellite performance for the long-lived event displayed low scatter correlation, overestimating both the total storm volume and the maximum volume intensity. Regarding the spatiotemporal characteristics, CMORPH and the weather radar shared the same orientation but differ in the maximum extension and the duration of the storm. CMORPH had a bigger extension with a longer duration (1 h) compared to the weather radar storm.

One of the main aims of an object-based approach is to decompose the total error into the sum of individual errors due to displacement, volume and pattern. The results obtained for the short-lived event indicate the pattern (aleatory error) the major error source, contributing 83%. This is followed by displacement, which contributed 13% to the total error. In the long-lived storm, volume and displacement contributed 47% and 50% of the total error, respectively.

5.1.2. Satellite error subtraction

After the storm objects were identified, errors in the satellite estimates due to location and magnitude were subtracted in the satellite data to create synthetic storm scenarios. To illustrate the spatial distribution of the storm scenarios over the Capivari catchment, Fig. 4 presents the total storm maps and the rainfall accumulation over the river streams based on radar, CMORPH and synthetic storm scenarios for the short-lived storm while Fig. 5 describes the corresponding maps for the long-lived storm event. The results for the short-lived storm scenario highlights the overestimation of CMORPH, in the upstream

Table 2
Performance criteria of model calibration and validation at different stations based on NSE, RMSE and R.

Station	Campinas		Monte		Outlet	
	Calibration	Validation	Calibration	Validation	Calibration	Validation
NSE	0.78	0.54	0.61	0.58	0.73	0.52
RMSE	3.52	2.57	6.17	8.99	16.23	19.98
R	0.89	0.76	0.81	0.77	0.91	0.72

area of the catchment. The location error scenario displaced the storm event to the northwest of the catchment, smoothing the rainfall excess of the storm event. The storm scenario due to magnitude scenario considerably reduced the overestimation in CMORPH, decreasing the total volume in the upstream area. The scenario for the long-lived storm event (Fig. 5) showed a significant rainfall overestimation in the northwestern part of the catchment, affecting the middle and lower areas. The location scenario slightly adjusted the storm event in the northwest, reducing the rainfall excess of the upstream area. However, this scenario still overestimated rainfall in the middle part of the catchment. Lastly, the magnitude storm error scenario effectively reduced extreme rainfall, overestimating rainfall over the catchment at small scales.

5.2. Hydrological impact

The hydrological response of systematic error due to location and

magnitude was analysed over three zones along the catchment: Upper (Campinas), Middle (Monte), and Lower (Outlet). Figs. 6 and 7 present the hydrological effect of systematic errors in CMORPH for the short- and long-lived scenarios using the hydrological simulation based on the radar storm for reference. In order to achieve a better description of the hydrological impact, hydrographs have been normalised with respect to the peak volume, Q_p , and the peak time, t_p , according to $(Q - Q_{min})/Q_p$ and t/t_p . Table 3 summarises the evaluation of hydrological impact to the location and the magnitude scenarios in the streamflow along the catchment based on r , $RMSE$, $MAPTE$, PPE and PVE .

The results for the short-lived storm event (Fig. 6) suggest that the overestimation of CMORPH in the rainfall storm consequently increased the streamflow volume over the catchment. The upper and lower areas, corresponding to Campinas and Monte, showed overestimation in the total volume of the storm of 70% and 40%, respectively, as a consequence of the notable overestimation of the peak flow. On the contrary, in the Outlet area, the level of overestimation was

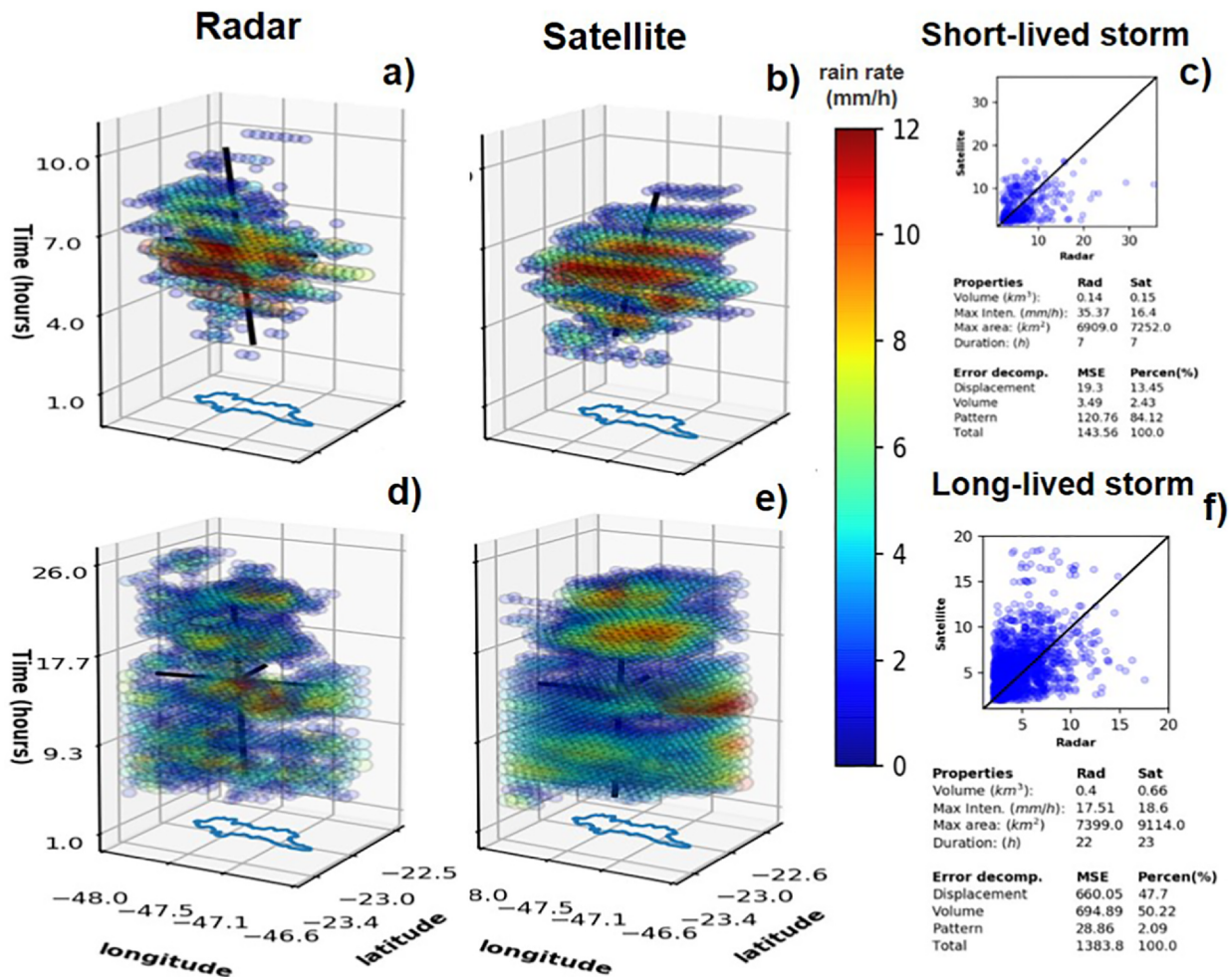


Fig. 3. object structure and storm error properties of the reference Radar and the satellite-based CMORPH identified by ST-CORA. a), b), c) short-lived storm and d), e), f) long-lived storm events.

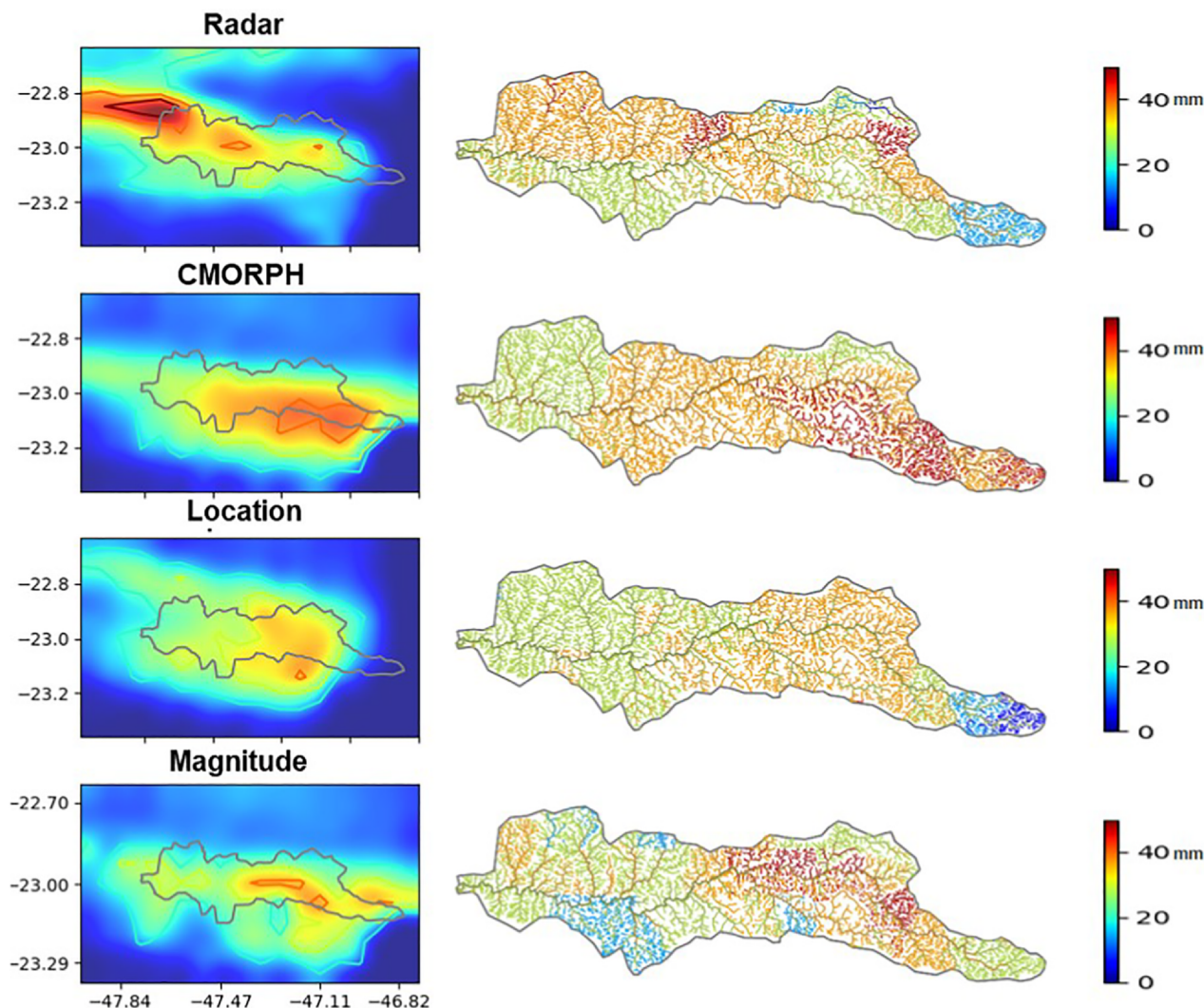


Fig. 4. Total event maps and rainfall accumulation by RADAR, CMORPH and synthetic storm scenarios for short-lived storm.

minimal, just 3% of the volume. Regarding the systematic errors, both scenarios decreased the streamflow volume and slightly increased the streamflow correlation over the catchment. The location scenario presented an important decrease of RMSE in Campinas and Monte. However, the RMSE was high in the Outlet area due to the underestimation by 4% of the streamflow volume. Regarding the hydrological effect in the temporal response of the storm, location and magnitude scenarios had an impact in the peak delay of 1 h at Monte, and 1–3 h at Outlet.

The hydrological response for the long-lived storm event (Fig. 7) is marked by the significant effect of the rainfall overestimation by CMORPH over the catchment. CMORPH systematically over-predicted stream-flow in Campinas, Monte and Outlet by 138%, 86% and 26%, respectively. The systematic error scenarios reduced the peak flow excess and consequently the RMSE in Campinas and Monte. However, the location did not affect the Outlet volume streamflow error. The location scenario had an important impact in Campinas, displaying the smallest RMSE and the higher *r*. On the other hand, The magnitude scenario was more relevant in Monte and especially in Outlet, which had a small RMSE and higher *r*. According to the MAPTE, the hydrological response showed a systematic delay of the peak in CMORPH as much as 3 h in Monte and 1 h in Outlet. The location scenario did not seem to impact on time delay, but the magnitude scenario exhibited a 1 h additional delay in Monte and zero delay in Outlet.

5.3. Streamflow error comparison

Fig. 8 describes the dispersion of the error variation corresponding to CMORPH and location and magnitude streamflow scenarios for short-lived (Fig. 8) and long-lived storm (Fig. 8b) events. Boxes represent the error variation dispersion between 25 and 75 percentiles and dots represent values outside the 99.9% percentile (back lines). positive percentile represents flow overestimation while negative percentile represents underestimation. Based on the results, overestimation prevails for both storm events over the catchment. In the short-lived storm, the location scenario displayed the lowest error variation (closest to zero), while the magnitude scenario showed the smallest variation in the long-lived storm. These results demonstrate that the error due to location in CMORPH had a dominant influence on the hydrological response of short-lived storm events. Meanwhile, error due to magnitude had a bigger influence in the hydrological response of the long-lived storm event.

6. Discussion

In the previous sections, we showed the evaluation of the impact of two systematic sources of error in CMORPH on the hydrological response in the Capivari catchment, Brazil. By using the ST-CORA method, we described the spatiotemporal characteristics of two meteorological storm events. Differences between physical properties of

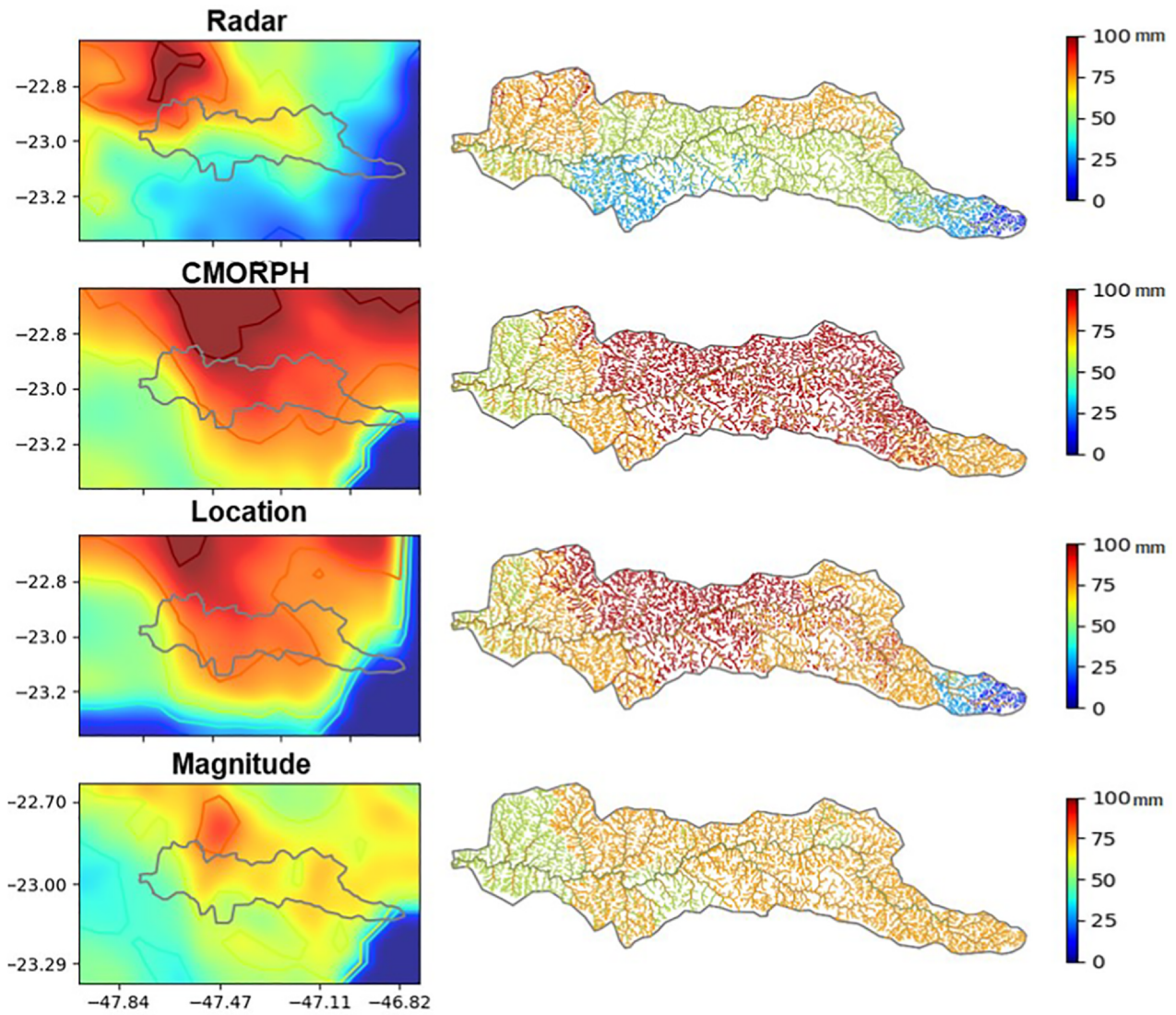


Fig. 5. Total event maps and rainfall accumulation by RADAR, CMORPH and synthetic storm scenarios for long-lived storm.

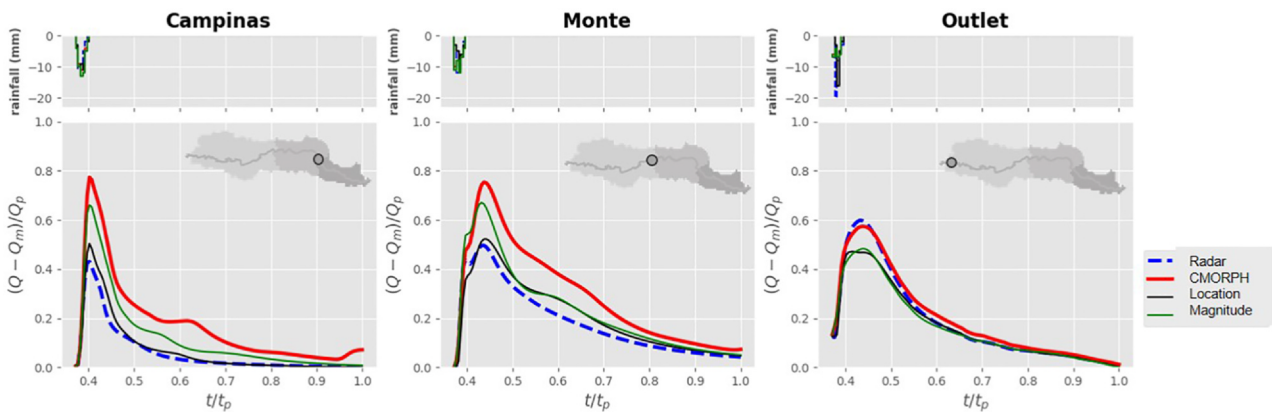


Fig. 6. hydrological response for short-live storm. Upper plots represent the rainfall hietograms and lower plots represent the corresponding discharges for Campinas, Monte and outlet zones.

observed and estimated objects allowed for the subtraction of two types of error: due to location and magnitude. Corresponding systematic scenarios were later propagated through a calibrated hydrological model to evaluate the individual hydrological impact of each source of error. In comparison to analytical approaches, this method analyses the

error decomposition independently of the hydrological model configuration.

The results indicate that CMORPH overestimates the total volume of both storm events, in agreement with multiple findings in South America (Ebert et al., 2007; Demaria et al., 2011; Laverde-Barajas et al.,

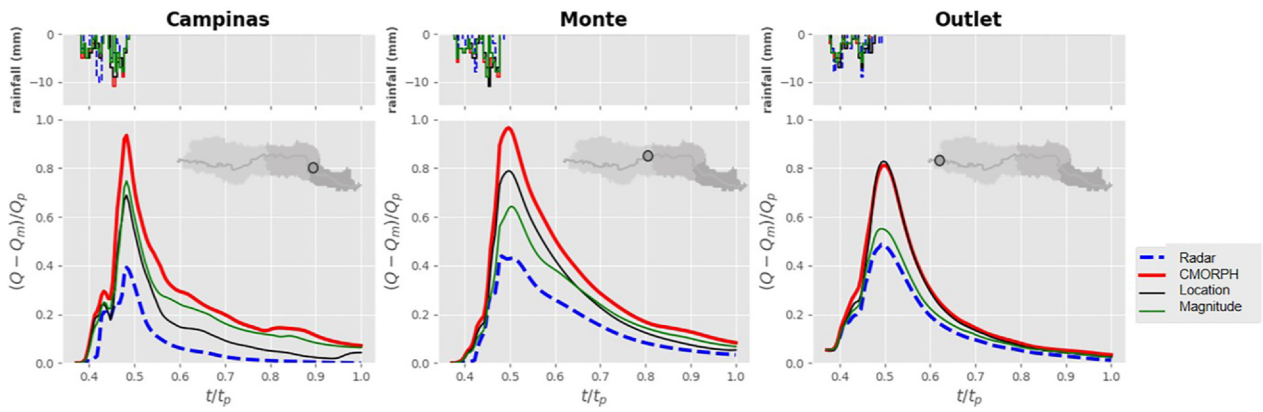


Fig. 7. hydrological response for long-lived storm. Upper plots represent the rainfall hietograms and lower plots represent the corresponding discharges for Campinas, Monte and outlet zones.

Table 3

Hydrological response evaluation for short and long-lived storm at Campinas, Monte and Outlet zones corresponding to Original, Location and Magnitude scenarios.

Storm type	Statistical index	Campinas			Monte			Outlet		
		Org	Location	Magnitude	Org	Location	Magnitude	Org	Location	Magnitude
Short-lived storm	r	0.964	0.991	0.986	0.974	0.974	0.994	0.997	0.995	0.996
	RMSE (mm)	4.99	0.89	2.92	7.03	2.17	3.39	5.91	11.70	12.08
	MAPTE (h)	0	0	0	0	1	1	1	3	1
	PPE (%)	(64.40)	(13.80)	(43.20)	(44.88)	(4.63)	(30.38)	2.63	13.53	12.36
	PVE (%)	(68.59)	(6.26)	(34.78)	(41.84)	(9.23)	(18.80)	(2.67)	3.47	3.89
long-lived storm	R	0.938	0.961	0.938	0.992	0.993	0.991	0.996	0.990	0.999
	RMSE (mm)	12.60	6.16	8.79	25.69	16.84	11.31	73.71	71.71	18.90
	MAPTE (h)	0.00	0.00	0.00	3.00	3.00	4.00	1.00	1.00	0.00
	PPE (%)	(118.58)	(64.76)	(77.62)	(111.54)	(74.15)	(43.21)	(49.46)	(51.99)	(9.83)
	PVE (%)	(137.92)	(59.06)	(99.22)	(86.40)	(51.86)	(41.94)	(26.22)	(22.76)	(7.97)

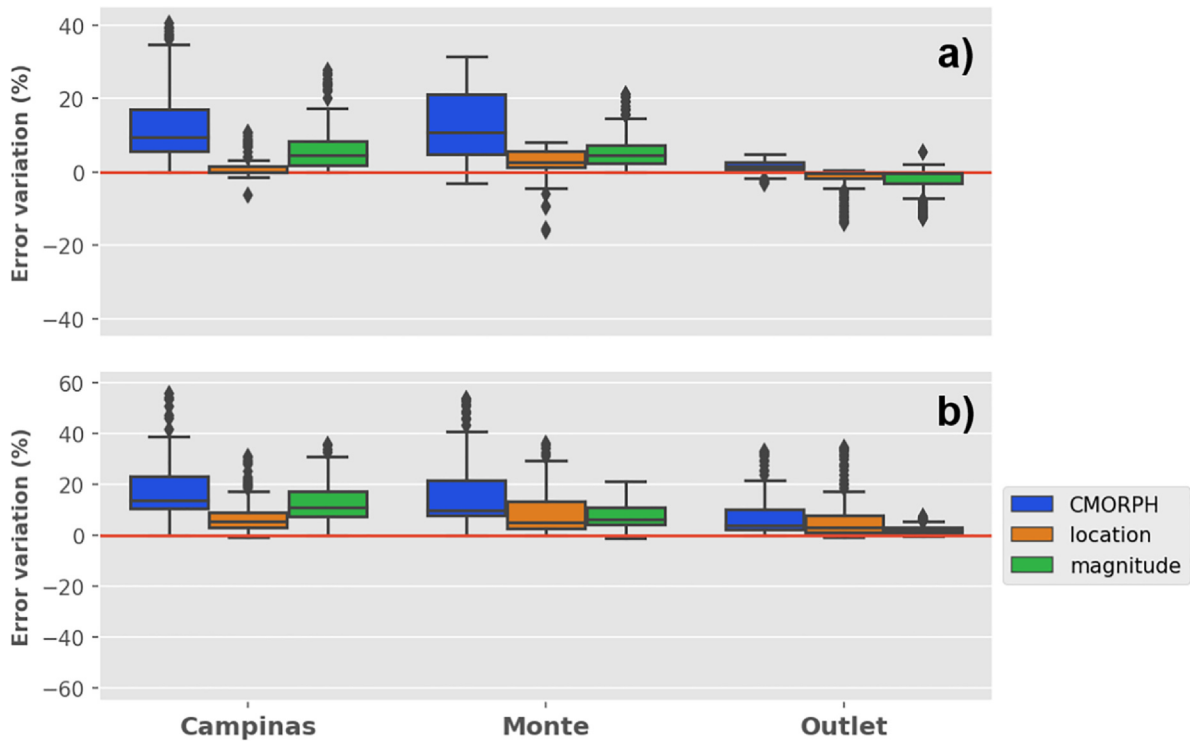


Fig. 8. Boxplots of the error distribution contribution for the original CMORPH event and location and magnitude stream-flow scenarios. a) Short-lived storm b) long-lived storm.

2018). Aleatory errors exhibited an important error component in CMORPH, especially in the short-lived storm event, where it represented almost 85% of the total error. Regarding systematic errors, location was found to be the main source of error for the short-lived storm events, while magnitude had a bigger influence on the long-lived storm event. In relation to the storm structure, errors CMORPH for the short-lived event are mainly attributed to the description of the storm orientation. In the case of the long-lived event those are a mainly focused to the spatiotemporal dimension of the storm. Despite that, these results do not represent the general performance of CMORPH for different storm types, these findings provide a framework to analyse the systematic error as a function of the type of storm event.

Regarding the hydrological response, the systematic overestimation by the satellite consequently lead to a large excess in the streamflow over the catchment. Errors in CMORPH due to location had a stronger effect on the short-lived storm mainly delaying between 1 and 3 h the time of the flow peak along catchment. In the analysis, the RMSE due to location decreased by 70% and 80% RMSE in the upper and middle zones, respectively. Results in the long-lived event showed that location subtraction had a low influence in the hydrological response. For this event, the location subtraction slightly reduced the streamflow volume in Campinas and Monte corresponding to elevated medium altitude areas and delaying 1 h peak flow of the streamflow in the area of outlet. On the other hand, Errors in CMORPH due to volume were more important for the long-lived storm. In all three zones, the reduction in rainfall volume directly impacted the decrease in streamflow excess. This reduction was especially important in Campinas and Monte slightly affecting the peak time of the stream flow in both areas. For the short-live event, the volume scenario marginally reduced the streamflow in all three areas and it had a small impact in the delay of the peakflow in Monte. These results suggest that there is a strong correlation between systematic errors inside satellite-based products and the streamflow properties, which are also found in similar studies using analytical approaches [e.g.] Zoccatelli et al. (2011), Mei et al. (2017)

We acknowledge certain limitations in the presented study. Firstly, the error in the hydrological model was not considered as an integral part of this research. Errors associated with modelling rainfall-runoff process were reduced by the use of an intense optimisation process to calibrate the hydrological model over the catchment. Another limitation to take into account arises from the sensitivity rainfall intensity threshold and the Critical Mass Threshold for the identification and the segmentation of storm objects. The characterisation parameters used in ST-CORA have potential implications for the storm definition and segmentation. Laverde-Barajas et al. (2019) showed the sensitivity analysis of the Critical Mass threshold used for delineating the storm object. Further studies could implement more sophisticated segmentation algorithms, such as multi-variable kernel segmentation or convolutions methods, to delineate the storm event.

7. Conclusions

In this study, we used the spatiotemporal object-based verification method, ST-CORA, to evaluate the hydrological impact of location and magnitude errors in CMORPH for storm estimation. The results obtained using a calibrated hydrological model of the Capivari river to reveal the main sources of systematic errors for short-lived and long-lived storm events. The most important conclusions of this study include the following:

1. Storm events described as objects using ST-CORA provided a unique perspective to characterise the main spatiotemporal characteristics of the storm in the catchment. Based on this information, differences between satellite and observed objects are calculated by separating the total error into three types: displacement, volume and pattern.
2. This study established location as the main source of systematic

error in the short-lived storm, while volume was identified as the main source in long-lived storm event. These errors significantly impacted the shape phase and amplitude of the streamflow hydrograph. In the short-lived storm, the subtraction of location error positively affected the error reduction in the upper and middle zones. In the long-lived storm, the subtraction of magnitude error in the storm event lead to an error reduction over all three zones in the catchment.

3. This study presented a better understanding of the spatiotemporal characteristics of the systematic errors in satellites for storm estimation and the impact in the hydrological response. However, errors relating to the hydrological model needs to be taken into account the potential “equifinality” of the optimal parameters used in the model.

4. Further research will incorporate the ST-CORA to improve the accuracy of satellite-based products in storm detection. Location and magnitude error subtraction methods can be incorporated into bias correction approaches for reducing the systematic error of near-real time satellite products in space and time. Additional satellite-based rainfall datasets can also be evaluated using the methodology for example, the GPM-IMERG satellite-based product (Huffman et al., 2015) or the Climate Hazards Group Infrared Precipitation with Station datasets (CHIRPS) (Funk et al., 2015).

CRedit authorship contribution statement

M. Laverde-Barajas: Conceptualization, Methodology, Software, Writing - original draft. **G.A. Corzo Perez:** Conceptualization, Methodology, Writing - original draft, Supervision. **F. Chishtie:** Writing - original draft. **A. Poortinga:** Writing - original draft. **R. Uijlenhoet:** Supervision. **D.P. Solomatine:** Conceptualization, Supervision.

Declaration of Competing Interest

The authors declare that they have no known competing financial interests or personal relationships that could have appeared to influence the work reported in this paper.

Acknowledgement

This work is part of a PhD study of the first author and was partially funded by the Colombian Administrative Department of Science, Technology and Innovation (COLCIENCIAS) under Grant number 646. The first author would also like to thank Prof. Wim Bastiaanssen from IHE and TUDelft for the additional financial support given. The authors would like to acknowledge the Universidade Estadual Paulista (UNESP) and the Agronomic Institute CIIAGROeFUNDAG Sao Paulo State Government for providing information of the weather radar station Barau and the hourly data from the automatic weather stations. Additionally, we would like to thank the Agency of the Piracicaba, Capivari and Jundiai Rivers (Agencia das Bacias PCJ) for the hourly streamflow data and also the agencies responsible for the satellite database used in this research. This work was carried out using the Dutch national e-infrastructure with the support of SURF Cooperative.

References

- Abdi, H., Williams, L.J., 2010. Principal component analysis. *Wiley Interdisc. Rev. Comput. Stat.* 2, 433–459.
- Abtew, W., 1996. Evapotranspiration measurements and modeling for three wetland systems in south florida. *JAWRA J. Am. Water Resour. Assoc.* 32, 465–473.
- Acharya, T., Ray, A.K., 2005. *Image Processing: Principles and Applications*. John Wiley & Sons.
- Amorati, R., Alberoni, P.P., Fornasiero, A., 2012. Operational bias correction of hourly radar precipitation estimate using rain gauges. In: *The 7th European Conference on Radar in Meteorology and Hydrology (ERAD)*.
- Artan, G., Gadain, H., Smith, J.L., Asante, K., Bandaragoda, C.J., Verdin, J.P., 2007. Adequacy of satellite derived rainfall data for stream flow modeling. *Nat. Haz.* 43,

- 167–185.
- Baldwin, M.E., Kain, J.S., 2006. Sensitivity of several performance measures to displacement error, bias, and event frequency. *Weather Forecast.* 21, 636–648.
- Bennett, N.D., Croke, B.F., Guariso, G., Guillaume, J.H., Hamilton, S.H., Jakeman, A.J., Marsili-Libelli, S., Newham, L.T., Norton, J.P., Perrin, C., et al., 2013. Characterising performance of environmental models. *Environ. Model. Software* 40, 1–20.
- Bitew, M.M., Gebremichael, M., 2011. Evaluation of satellite rainfall products through hydrologic simulation in a fully distributed hydrologic model. *Water Resour. Res.* 47.
- Boers, N., Bookhagen, B., Marwan, N., Kurths, J., 2015. Spatiotemporal characteristics and synchronization of extreme rainfall in south america with focus on the andes mountain range, 46, 601–617. URL:<http://link.springer.com/article/10.1007/s00382-015-2601-6>.
- Bui, Y.T., Orange, D., Visser, S., Hoanh, C.T., Laissus, M., Poortinga, A., Tran, D.T., Stroosnijder, L., 2014. Lumped surface and sub-surface runoff for erosion modeling within a small hilly watershed in northern vietnam. *Hydrol. Process.* 28, 2961–2974.
- Cannon, A.J., Sobie, S.R., Murdoch, T.Q., 2015. Bias correction of gcm precipitation by quantile mapping: How well do methods preserve changes in quantiles and extremes? *J. Clim.* 28, 6938–6959. <https://doi.org/10.1175/JCLI-D-14-00754.1>. URL:<https://doi.org/10.1175/JCLI-D-14-00754.1> arXiv:<https://doi.org/10.1175/JCLI-D-14-00754.1>.
- Casati, B., Wilson, L., Stephenson, D., Nurmi, P., Ghelli, A., Pocerich, M., Damrath, U., Ebert, E., Brown, B., Mason, S., 2008. Forecast verification: current status and future directions. *Meteorol. Appl. J. Forecast., Pract. Appl. Techn. Model.* 15, 3–18.
- Casse, C., Gosset, M., Peugeot, C., Pedinotti, V., Boone, A., Tanimoun, B., Decharme, B., 2015. Potential of satellite rainfall products to predict niger river flood events in niamey. *Atmos. Res.* 163, 162–176.
- Ceperuelo, M., Llasat, M., Rigo, T., 2006. Rainfall events and hailstorms analysis program (rhap). *Adv. Geosci.* 7.
- Chen, F., Yang, X., Ji, C., Li, Y., Deng, F., Dong, M., 2019. Establishment and assessment of hourly high-resolution gridded air temperature data sets in zhejiang, china. *Meteorol. Appl.* 26, 396–408.
- Chung, U., Yun, J.I., 2004. Solar irradiance-corrected spatial interpolation of hourly temperature in complex terrain. *Agric. Forest Meteorol.* 126, 129–139.
- Corzo Perez, G.A., van Huijgevoort, M.H.J., Voß, F., van Lanen, H.A.J., 2011. On the spatio-temporal analysis of hydrological droughts from global hydrological models. *Hydrol. Earth Syst. Sci.* 15, 2963–2978. <https://doi.org/10.5194/hess-15-2963-2011>. URL:<https://www.hydrol-earth-syst-sci.net/15/2963/2011/>.
- Davis, C.A., Brown, B., Bullock, R., 2009. Spatial and temporal object-based evaluation of numerical precipitation forecasts. In: Preprints, 23rd Conf. on Weather Analysis and Forecasting/19th Conf. on Numerical Weather Prediction, Omaha, NE, Amer. Meteor. Soc. A, vol. 5.
- DeGaetano, A.T., Belcher, B.N., 2007. Spatial interpolation of daily maximum and minimum air temperature based on meteorological model analyses and independent observations. *J. Appl. Meteorol. Climatol.* 46, 1981–1992.
- Demaria, E., Rodriguez, D., Ebert, E., Salio, P., Su, F., Valdes, J.B., 2011. Evaluation of mesoscale convective systems in south america using multiple satellite products and an object-based approach. *J. Geophys. Res. Atmos.* 116.
- Dinku, T., Ruiz, F., Connor, S.J., Ceccato, P., 2010. Validation and intercomparison of satellite rainfall estimates over colombia. *J. Appl. Meteorol. Climatol.* 49, 1004–1014.
- DSMW-FAO, 1960. Fao digital soil map of the world. URL:<http://www.fao.org/land-water/land/land-governance/land-resources-planning-toolbox/category/details/en/c/1026564/>.
- Ebert, E., McBride, J., 2000. Verification of precipitation in weather systems: determination of systematic errors. *J. Hydrol.* 239, 179–202.
- Ebert, E.E., Gallus, W.A., 2009. Toward better understanding of the contiguous rain area (CRA) method for spatial forecast verification. 24, 1401–1415. URL:<http://journals.ametsoc.org/doi/abs/10.1175/2009WAF2222252.1>.
- Ebert, E.E., Janowiak, J.E., Kidd, C., 2007. Comparison of near-real-time precipitation estimates from satellite observations and numerical models. *Bull. Am. Meteorol. Soc.* 88, 47–64.
- Ehret, U., Zehe, E., 2011. Series distance-an intuitive metric to quantify hydrograph similarity in terms of occurrence, amplitude and timing of hydrological events. *Hydrol. Earth Syst. Sci.* 15.
- Falck, A.S., Maggioni, V., Tomasella, J., Vila, D.A., Diniz, F.L., 2015. Propagation of satellite precipitation uncertainties through a distributed hydrologic model: a case study in the tocantins-araguaia basin in Brazil. *J. Hydrol.* 527, 943–957. <https://doi.org/10.1016/j.jhydrol.2015.05.042>. URL:<http://www.sciencedirect.com/science/article/pii/S0022169415003923>.
- Funk, C., Peterson, P., Landsfeld, M., Pedreros, D., Verdin, J., Shukla, S., Husak, G., Rowland, J., Harrison, L., Hoell, A., et al., 2015. The climate hazards infrared precipitation with stations: a new environmental record for monitoring extremes. *Sci. Data* 2, 150066.
- Gash, J.H., Lloyd, C., Lachaud, G., 1995. Estimating sparse forest rainfall interception with an analytical model. *J. Hydrol.* 170, 79–86.
- Geem, Z.W., Kim, J.H., Loganathan, G.V., 2001. A new heuristic optimization algorithm: harmony search. *Simulation* 76, 60–68.
- Grams, J.S., Gallus Jr, W.A., Koch, S.E., Wharton, L.S., Loughe, A., Ebert, E.E., 2006. The use of a modified ebert-mcbride technique to evaluate mesoscale model qpf as a function of convective system morphology during ihop 2002. *Weather Forecast.* 21, 288–306. <https://doi.org/10.1175/WAF918.1>. URL:<https://journals.ametsoc.org/doi/abs/10.1175/WAF918.1>.
- Guo, H., Chen, S., Bao, A., Hu, J., Gebregiorgis, A.S., Xue, X., Zhang, X., 2015. Inter-comparison of high-resolution satellite precipitation products over Central Asia. *Remote Sens.* 7, 7181–7211. <https://doi.org/10.3390/rs70607181>. URL:<http://www.mdpi.com/2072-4292/7/6/7181>.
- Han, L., Fu, S., Zhao, L., Zheng, Y., Wang, H., Lin, Y., 2009. 3d convective storm identification, tracking, and forecasting-an enhanced TITAN algorithm. 26, 719–732. URL:<https://journals.ametsoc.org/doi/abs/10.1175/2008JTECHA1084.1>.
- Hoffman, R.N., Liu, Z., Louis, J.-F., Grassotti, C., 1995. Distortion representation of forecast errors. *Mon. Weather Rev.* 123, 2758–2770.
- Hossain, F., Anagnostou, E.N., 2006. A two-dimensional satellite rainfall error model. *IEEE Trans. Geosci. Remote Sens.* 44, 1511–1522.
- Hu, Z., Hu, Q., Zhang, C., Chen, X., Li, Q., 2016. Evaluation of reanalysis, spatially interpolated and satellite remotely sensed precipitation data sets in Central Asia. *J. Geophys. Res. Atmos.* 121, 5648–5663. <https://doi.org/10.1002/2016JD024781>. URL:<http://onlinelibrary.wiley.com/doi/10.1002/2016JD024781/abstract>.
- Huffman, G.J., Bolvin, D.T., Nelkin, E.J., et al., 2015. Integrated multi-satellite retrievals for gpm (imerg) technical documentation. NASA/GSFC Code 612, 2019.
- IBGE, 2017. Monitoramento da cobertura e uso da terra: 2000–2010 – 2012–2014: em grade territorial estatística. 101469. Instituto Brasileiro de Geografia e Estatística. URL:<https://biblioteca.ibge.gov.br/visualizacao/livros/liv101469.pdf>.
- Johnson, A.E., Hebert, M., 1999. Using spin images for efficient object recognition in cluttered 3d scenes. *IEEE Trans. Pattern Anal. Mach. Intell.* 21, 433–449.
- Joyce, R.J., Janowiak, J.E., Arkin, P.A., Xie, P., 2004. Cmorph: a method that produces global precipitation estimates from passive microwave and infrared data at high spatial and temporal resolution. *J. Hydrometeorol.* 5, 487–503.
- Kidd, C., Becker, A., Huffman, G.J., Muller, C.L., Joe, P., Skofronick-Jackson, G., Kirschbaum, D.B., 2017. So, how much of the earth's surface is covered by rain gauges? *Bull. Am. Meteorol. Soc.* 98, 69–78.
- Laverde-Barajas, M., Corzo, G., Bhattacharya, B., Uijlenhoet, R., Solomatine, D.P., 2019. Spatiotemporal analysis of extreme rainfall events using an object-based approach. In: Corzo, G., Varouchakis, E.A. (Eds.), *Spatiotemporal Analysis of Extreme Hydrological Events*. Elsevier, pp. 95–112. <https://doi.org/10.1016/B978-0-12-811689-0.00005-7>. URL:<http://www.sciencedirect.com/science/article/pii/B9780128116890000057>.
- Laverde-Barajas, M., Corzo Perez, G., Dalfré Filho, J., Solomatine, D., 2018. Assessing the performance of near real-time rainfall products to represent spatiotemporal characteristics of extreme events: case study of a subtropical catchment in South-eastern Brazil. *Int. J. Remote Sens.* 39, 7568–7586. <https://doi.org/10.1080/101431161.2018.1475773>. URL:<https://doi.org/10.1080/101431161.2018.1475773>.
- Li, J., Hsu, K., AghaKouchak, A., Sorooshian, S., 2015. An object-based approach for verification of precipitation estimation. *Int. J. Remote Sens.* 36, 513–529. <https://doi.org/10.1080/01431161.2014.999170>. URL:<https://doi.org/10.1080/01431161.2014.999170>.
- Li, J., Hsu, K.-L., AghaKouchak, A., Sorooshian, S., 2016. Object-based assessment of satellite precipitation products. *Remote Sens.* 8, 547. <https://doi.org/10.3390/rs8070547>. URL:<http://www.mdpi.com/2072-4292/8/7/547>.
- Li, L., Hong, Y., Wang, J., Adler, R.F., Policelli, F.S., Habib, S., Irwin, D., Korme, T., Okello, L., 2009. Evaluation of the real-time trmm-based multi-satellite precipitation analysis for an operational flood prediction system in nozia basin, lake victoria, africa. *Nat. Haz.* 50, 109–123. <https://doi.org/10.1007/s11069-008-9324-5>. URL:<http://link.springer.com/article/10.1007/s11069-008-9324-5>.
- Maggioni, V., Massari, C., 2018. On the performance of satellite precipitation products in riverine flood modeling: a review. *J. Hydrol.* 558, 214–224. <https://doi.org/10.1016/j.jhydrol.2018.01.039>. URL:<http://www.sciencedirect.com/science/article/pii/S0022169418300398>.
- Maggioni, V., Sapiano, M.R., Adler, R.F., Tian, Y., Huffman, G.J., 2014. An error model for uncertainty quantification in high-time-resolution precipitation products. *J. Hydrometeorol.* 15, 1274–1292.
- Mei, Y., Anagnostou, E.N., Nikolopoulos, E.I., Borga, M., 2014. Error analysis of satellite precipitation products in mountainous basins. *J. Hydrometeorol.* 15, 1778–1793. <https://doi.org/10.1175/JHM-D-13-0194.1>. URL:<http://journals.ametsoc.org/doi/abs/10.1175/JHM-D-13-0194.1>.
- Mei, Y., Anagnostou, E.N., Shen, X., Nikolopoulos, E.I., 2017. Decomposing the satellite precipitation error propagation through the rainfall-runoff processes. 109, 253–266. URL:<http://www.sciencedirect.com/science/article/pii/S0309170817301343>.
- Mei, Y., Nikolopoulos, E.I., Anagnostou, E.N., Zoccatelli, D., Borga, M., 2016. Error analysis of satellite precipitation-driven modeling of flood events in complex alpine terrain. *Remote Sens.* 8, 293. <https://doi.org/10.3390/rs8040293>. URL:<https://www.mdpi.com/2072-4292/8/4/293>.
- Mei, Y., Shen, X., Anagnostou, E.N., 2017. A synthesis of space-time variability in multicomponent flood response. *Hydrol. Earth Syst. Sci.* 21.
- Michaelides, S., Levizzani, V., Anagnostou, E., Bauer, P., Kasparis, T., Lane, J., 2009. Precipitation: measurement, remote sensing, climatology and modeling. *Atmos. Res.* 94, 512–533. <https://doi.org/10.1016/j.atmosres.2009.08.017>. URL:<http://www.sciencedirect.com/science/article/pii/S0169809509002488>.
- Mittermaier, M.P., Bullock, R., 2013. Using MODE to explore the spatial and temporal characteristics of cloud cover forecasts from high-resolution NWP models, 20, 187–196.
- Molini, L., Parodi, A., Rebora, N., Craig, G.C., 2011. Classifying severe rainfall events over italy by hydrometeorological and dynamical criteria, 137, 148–154. URL:<http://onlinelibrary.wiley.com/doi/10.1002/qj.741/abstract>.
- Molini, L., Parodi, A., Siccardi, F., 2009. Dealing with uncertainty: an analysis of the severe weather events over italy in 2006. *Nat. Haz. Earth Syst. Sci.* 9, 1775–1786.
- Nash, J.E., Sutcliffe, J.V., 1970. River flow forecasting through conceptual models part i—a discussion of principles. *J. Hydrol.* 10, 282–290.
- Nikolopoulos, E.I., Anagnostou, E.M., Borga, M., 2013. Using High-Resolution Satellite Rainfall Products to Simulate a Major Flash Flood Event in Northern Italy. *J. Hydrometeorol.* 14, 171–185. <https://doi.org/10.1175/JHM-D-12-09.1>.
- Paiva, R.C., Durand, M.T., Hossain, F., 2015. Spatiotemporal interpolation of discharge across a river network by using synthetic swot satellite data. *Water Resour. Res.* 51,

- 430–449.
- Peleg, N., Marra, F., Fatichi, S., Paschalis, A., Molnar, P., Burlando, P., 2018. Spatial variability of extreme rainfall at radar subpixel scale. *J. Hydrol.* 556, 922–933. <https://doi.org/10.1016/j.jhydrol.2016.05.033>. URL:<http://www.sciencedirect.com/science/article/pii/S0022169416303006>.
- Perez, R.E., Jansen, P.W., Martins, J.R., 2012. pyopt: a python-based object-oriented framework for nonlinear constrained optimization. *Struct. Multidisc. Optim.* 45, 101–118.
- Phongsapan, K., Chishtie, F., Poortinga, A., Bhandari, B., Meechaiya, C., Kunlamai, T., Aung, K.S., Saah, D., Anderson, E., Markert, K., et al., 2019. Operational flood risk index mapping for disaster risk reduction using earth observations and cloud computing technologies: a case study on myanmar. *Front. Environ. Sci.* 7, 191.
- Poortinga, A., Bastiaanssen, W., Simons, G., Saah, D., Senay, G., Fenn, M., Bean, B., Kadyszewski, J., 2017. A self-calibrating runoff and streamflow remote sensing model for ungauged basins using open-access earth observation data. *Remote Sens.* 9, 86.
- Qiao, L., Hong, Y., Chen, S., Zou, C.B., Gourley, J.J., Yong, B., 2014. Performance assessment of the successive version 6 and version 7 tmpa products over the climate-transitional zone in the southern great plains, USA. *J. Hydrol.* 513, 446–456.
- Sapiano, M., Arkin, P., 2009. An intercomparison and validation of high-resolution satellite precipitation estimates with 3-hourly gauge data. *J. Hydrometeorol.* 10, 149–166.
- Saulnier, G.-M., Le Lay, M., 2009. Sensitivity of flash-flood simulations on the volume, the intensity, and the localization of rainfall in the cévennes-vivarais region (France). *Water Resour. Res.* 45.
- Schellekens, J., van Verseveld, W., Visser, M., Winsemius, H., Euserand, T., Bouaziz, L., C, T., de Vriesand, s., Boisgontierand, H., Eilanderand, D., Tollenaarand, D., Weertsand, A., Baartand F, P., Hazenbergand, Lutz, L., ten Velden, C., Jansen, M., & Benedict, M., 2018. Wflow, openstreams/wflow: unstable-master. OpenStream wflow documentation release, doi: <https://doi.org/10.5281/zenodo.593510>.
- SEDEC, 2013. Secretaria nacional de proteção e defesa civil, sistema integrado de informações sobre desastres – s2id. URL:<https://s2id.mi.gov.br/paginas/series> (accessed February, 2019).
- Sedgewick, R., 1998. Algorithms in C, Parts 1–4: Fundamentals, Data Structures, Sorting, Searching, (3rd ed.). Addison-Wesley Professional.
- Sellers, S., Nguyen, P., Chu, W., Gao, X., Hsu, K.-L., Sorooshian, S., 2013. Computational earth science: Big data transformed into insight, 94, 277–278.
- Skok, G., Tribbia, J., Rakovec, J., Brown, B., 2009. Object-based analysis of satellite-derived precipitation systems over the low-and midlatitude pacific ocean. *Mon. Weather Rev.* 137, 3196–3218. <https://doi.org/10.1175/2009MWR2900.1>. URL:<http://journals.ametsoc.org/doi/abs/10.1175/2009MWR2900.1>.
- Steiner, M., Houze Jr, R.A., Yuter, S.E., 1995. Climatological characterization of three-dimensional storm structure from operational radar and rain gauge data. *J. Appl. Meteorol.* 34, 1978–2007.
- Stisen, S., Sandholt, I., 2010. Evaluation of remote-sensing-based rainfall products through predictive capability in hydrological runoff modelling. *Hydrol. Process. Int. J.* 24, 879–891.
- Su, F., Hong, Y., Lettenmaier, D.P., 2008. Evaluation of trmm multisatellite precipitation analysis (tmpa) and its utility in hydrologic prediction in the la plata basin. *J. Hydrometeorol.* 9, 622–640.
- Sun, Q., Miao, C., Duan, Q., Ashouri, H., Sorooshian, S., Hsu, K.-L., 2018. A review of global precipitation data sets: data sources, estimation, and intercomparisons. *Rev. Geophys.* 56, 79–107. <https://doi.org/10.1002/2017RG000574>. URL:<http://doi.wiley.com/10.1002/2017RG000574>.
- Swiss, R., 2011. Flood risk in Brazil: prevention, adaptation and insurance. URL:<http://media.swissre.com/documents>.
- Tangune, B.F., Escobedo, J.F., 2018. Reference evapotranspiration in so paulo state: empirical methods and machine learning techniques. *Int. J. Water Resour. Environ. Eng.* 10, 33–44.
- Teng, J., Potter, N.J., Chiew, F.H.S., Zhang, L., Wang, B., Vaze, J., Evans, J.P., 2015. How does bias correction of regional climate model precipitation affect modelled runoff? *Hydrol. Earth Syst. Sci.* 19, 711–728. <https://doi.org/10.5194/hess-19-711-2015>. URL:<https://www.hydrol-earth-syst-sci.net/19/711/2015/>.
- Themeßl, M.J., Gobiet, A., Heinrich, G., 2012. Empirical-statistical downscaling and error correction of regional climate models and its impact on the climate change signal. *Clim. Change* 112, 449–468.
- Thiemig, V., Rojas, R., Zambrano-Bigiarini, M., Levizzani, V., De Roo, A., 2012. Validation of satellite-based precipitation products over sparsely gauged African River Basins. *J. Hydrometeorol.* 13, 1760–1783. <https://doi.org/10.1175/JHM-D-12-032.1>. URL:<http://journals.ametsoc.org/doi/abs/10.1175/JHM-D-12-032.1>.
- Tolentino, P.L.M., Poortinga, A., Kanamaru, H., Keesstra, S., Maroulis, J., David, C.P.C., Ritsema, C.J., 2016. Projected impact of climate change on hydrological regimes in the philippines. *PLoS One* 11, e0163941.
- Van Zyl, J.J., 2001. The shuttle radar topography mission (srtm): a breakthrough in remote sensing of topography. *Acta Astronaut.* 48, 559–565.
- Vergara, H., Hong, Y., Gourley, J.J., Anagnostou, E.N., Maggioni, V., Stampoulis, D., Kirstetter, P.-E., 2014. Effects of resolution of satellite-based rainfall estimates on hydrologic modeling skill at different scales. *J. Hydrometeorol.* 15, 593–613.
- Vertessy, R.A., Elsenbeer, H., 1999. Distributed modeling of storm flow generation in an amazonian rain forest catchment: Effects of model parameterization. *Water Resour. Res.* 35, 2173–2187.
- Viglione, A., Chirico, G.B., Komma, J., Woods, R., Borga, M., Blöschl, G., 2010. Quantifying space-time dynamics of flood event types. *J. Hydrol.* 394, 213–229.
- Wesselung, C.G., Karssenber, D.-J., Burrough, P.A., van Deursen, W.P., 1996. Integrating dynamic environmental models in gis: the development of a dynamic modelling language. *Trans. GIS* 1, 40–48.
- Yilmaz, K.K., Hogue, T.S., Hsu, K.-L., Sorooshian, S., Gupta, H.V., Wagener, T., 2005. Intercomparison of rain gauge, radar, and satellite-based precipitation estimates with emphasis on hydrologic forecasting. *J. Hydrometeorol.* 6, 497–517. <https://doi.org/10.1175/JHM431.1>. URL:<https://journals.ametsoc.org/doi/full/10.1175/JHM431.1>.
- Zoccatelli, D., Borga, M., Viglione, A., Chirico, G., Blöschl, G., 2011. Spatial moments of catchment rainfall: rainfall spatial organisation, basin morphology, and flood response. *Hydrol. Earth Syst. Sci.* 15, 3767.